Fast STEM Spectrum Imaging Using Simultaneous EELS and EDS

Paolo Longo* and Ray D Twesten
Gatan Inc., 5794 W Las Positas Blvd., Pleasanton, CA, 94588
*plongo@gatan.com

Introduction

Up to now, researchers performing analytical investigations in the transmission electron microscope typically had to choose between analytical spectroscopy techniques. They might choose energy dispersive X-ray spectroscopy (EDS) analysis when working with thick samples containing high-Z elements or choose electron energy-loss spectroscopy (EELS) when studying low-Z materials in thin samples [1]. With the advent of STEM instruments possessing both high-mechanical stability and high-brightness probes [2], coupled with the latest generation of fast, efficient X-ray and EELS detectors [3, 4], choosing between complementary techniques is a significant restriction. The acquisition systems available up to now have forced a choice because EELS, EDS, and fast scanning have not been designed to work together, resulting in inefficient data collection.

In this article, we present a data collection system that is designed to allow EELS, EDS, and dark field detectors to operate efficiently at spectral rates over 1 kHz. This is achieved by allowing each detector system to acquire data independent of the other. The data collection systems are, however, linked together by a synchronization clock pulse to ensure the resulting datasets are in exact spatial alignment. The system described here was recently implemented using DigitalMicrograph together with the Bruker Esprit EDS system. The necessary timing precision is achieved by synchronizing the EELS and the EDS spectrometers with the beam scanning system as shown schematically in Figure 1. During simultaneous spectral acquisition, the EELS spectrometer provides system synchronization by means of a clock pulse at the end of each acquired frame. This pulse is used to advance the beam position and to inform the EDS system that the pixel has advanced. The EELS and EDS data are stored locally in software buffers and transferred asynchronously to the host application to ensure no data is lost. This mode of acquisition can be performed with any combination of the available signals and is also compatible with other features such as DualEELS™ [3, 5, 6] acquisition and spatial drift correction.

Methods and Materials

To illustrate these advances, data was acquired at TU-Graz in Austria using a probe-corrected FEI Titan G3 STEM equipped with an X-FEG high-brightness electron source operating at 300 kV. The instrument is also equipped with a four-quadrant SDD detector (FEI Super-X) [4] controlled by the Bruker Esprit system and a GIF Quantum ERS imaging filter for EELS acquisition [3]. The EELS spectrometer is configured with the following features: (a) DualEELS™ capability, which allows two different regions of the EELS spectrum to be recorded nearly simultaneously (Δt = 10 µs); (b) a low-dispersion mode that allows EELS data to be recorded with an energy range up to 2000 eV (or 4000 eV in DualEELS mode); (c) a fast 2-k CCD sensor that allows EELS acquisition at over 1000 spectra per second; and (d) a dodecapole lens system capable of correcting spectral aberrations up to the 5th order, allowing collection angles well over 100 mrad to be used while maintaining sub-eV energy resolution.

The sample analyzed consisted of Pd/Au catalyst nanoparticles kindly provided by Professor Jianfang Wang's group at the Chinese University of Hong Kong. Pd-Au alloys have attracted a lot of interest because of their resistance to high temperatures, and this explains their use in several fields such as CO and hydrocarbon oxidation, the synthesis of vinyl acetate monomer, hydrocarbon hydrogenation, and many other reactions [7, 8]. Palladium is the catalytic center, whereas the Au has the effect of changing the catalytic properties at the surface of the Pd-Au alloy [9, 10]. TEM samples were prepared by depositing the catalyst particles onto a carbon film supported by a Cu mesh TEM grid.

Data was acquired using a 220 pA STEM probe as indicated by the current collected on microscope fluorescence screen. The STEM is capable of much higher

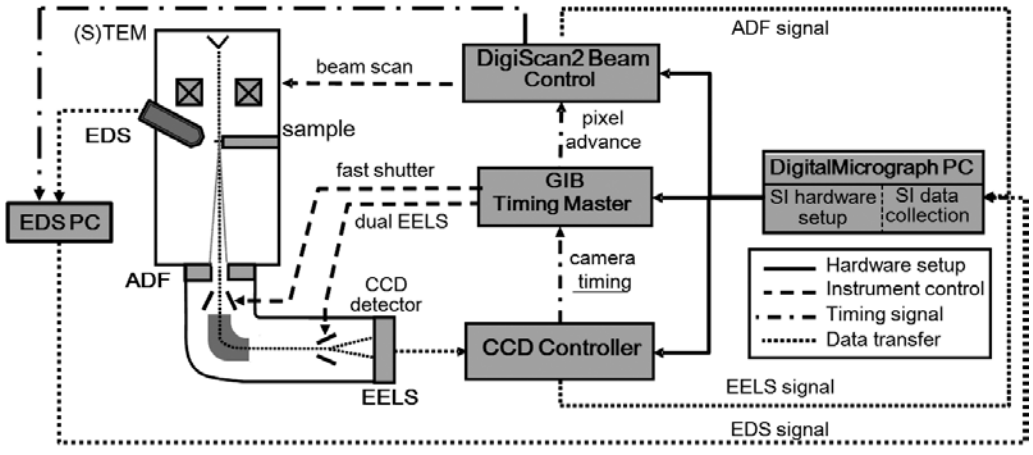

Figure 1: Control signal and data path for joint high-speed EELS and EDS data acquisition. Hardware setup and data transfer are handled asynchronously while instrument control and timing signals are controlled via a master timing system, ensuring all data stays in perfect synchrony and no data are lost.

 doi:10.1017/S1551929512000909

currents, but a relatively low current was needed to minimize sample motion caused by local heating. The probe convergence angle was 20 mrad, and the collection angle was 35 mrad. Four different signals (ADF, EDS, EELS high core loss, and low-energy core loss) were recorded simultaneously. The EELS spectrum image (SI) was acquired in DualEELS™ mode; the regions of the EELS spectrum from 200 eV to 2200 eV and 1800 eV to 3800 eV were acquired using acquisition times of 7 ms and 30 ms, respectively. EDS spectra were acquired simultaneously, integrating counts over the entire pixel time employed for the EELS acquisition. The resulting EDS pixel time was 39 ms at nearly 100% live time. The X-ray count rate was approximately 15k counts/s in the center of a typical Au particle.

Results

Figures 2b–2d show EDS and EELS spectra from a single pixel extracted from the region shown in Figure 2a. The EELS spectra show a good amount of signal; the Au $M_{4,5}$-edges at 2206 eV stand out well above the background, and a small amount of Pd is evident. The EDS data shows Au X rays as well as Cu fluorescence from the support grid.

The quality of the spectra for both EELS and EDS dramatically improves after summing adjacent pixels together as shown in Figures 3b–3d where 168 pixels across the region shown in Figure 3a were summed. In the summed EDS spectrum, the lines for all the elements present in the sample are observed. Moreover, the lack of a Cu $L_{2,3}$-edges at 931 eV in the EELS data verifies the nature of the EDS artifact peak from the Cu grid. The EELS low and high core-loss spectra appear to be virtually noiseless because of the high number of counts in the data. The Pd $M_{4,5}$-edges at 335 eV appear to be strong, as well as the Au $M_{4,5}$-edges at 2206 eV in the high core-loss spectrum. It is also interesting to note there is sufficient signal in the summed EELS data that even the high-energy Pd $L_{2,3}$-edges at 3170 eV are above the background level and can be used for analysis if needed as described elsewhere [11].

These results demonstrate that when the EELS system and STEM are properly configured, high-energy edges can be recorded with good signal-to-noise ratio using short exposure times. This illustrates the suitability of EELS as a technique to analyze materials containing heavy metals such as Au.

Figures 4a and 4b show for the same specimen region Pd elemental maps by EDS and EELS, respectively. In the case of EDS, the map was extracted from the L_α lines at 2.84 keV using an empirical Kramers background [12] fitting followed by multiple linear least square (MLLS) fitting of each peak represented by a set of Gaussian peaks. In the EELS case, the Pd $M_{4,5}$-edges at 335 eV were used. The signal overlap with C K-edge of the underlying support film at 284 eV is easily separated using MLLS fitting. MLLS curve fitting of the overlap is only possible when the signal-to-noise ratio for each individual pixel is sufficiently high, as is the case in these EELS data [13, 14, 15]. The EELS elemental map for the Pd looks much sharper and shows higher contrast than the same map obtained using EDS. This can be directly attributed to the strong forward scattering of the EELS signal and the nearly 100% collection efficiency of the detector [3]. The high signal-to-noise ratio in the data is evident from the intensity line profiles shown in Figure 5, where profiles were produced from 5-pixel-wide averages along the red boxes of Figure 4.

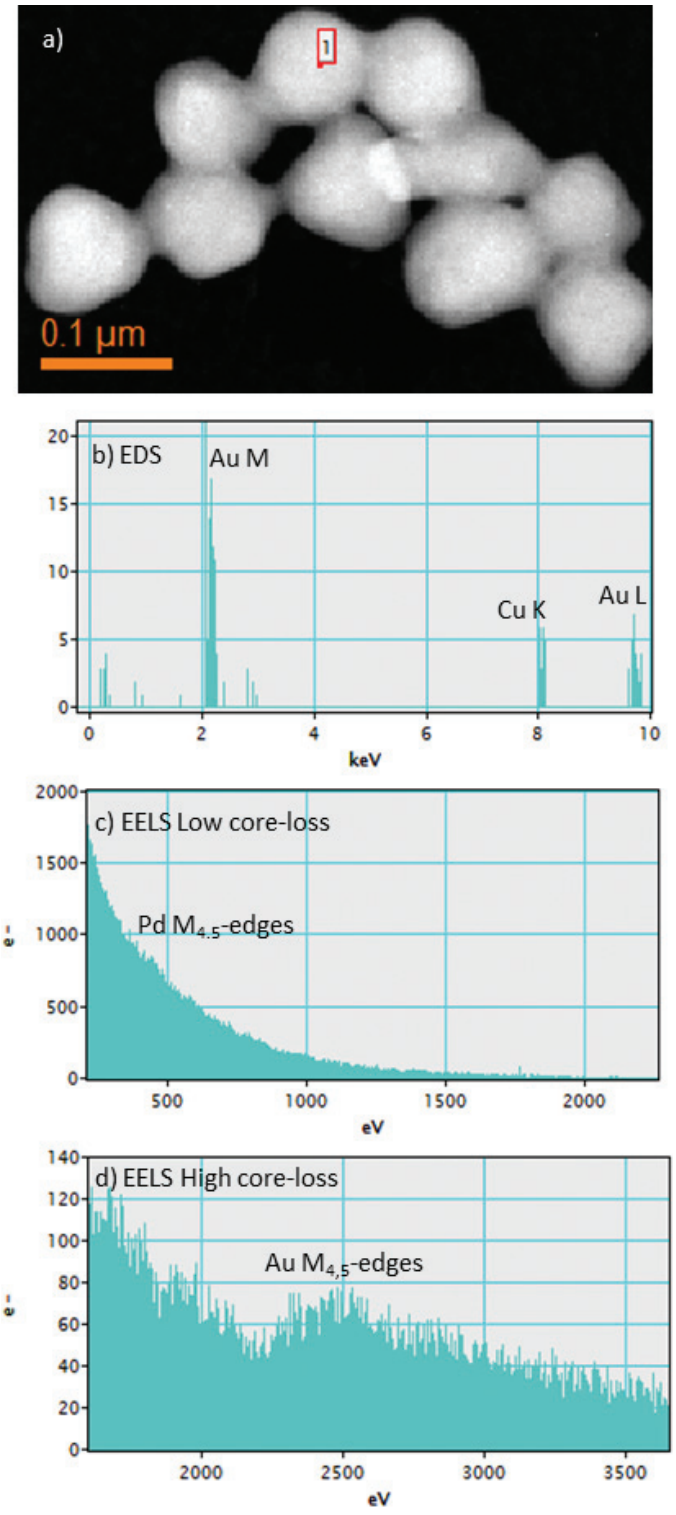

Figure 2: (a) ADF image acquired simultaneously with the EELS and EDS data showing the location of a single extracted data point. (b) EDS data from selected point, (c) low core loss, and (d) high core loss EELS data from the same point. The EELS data indicated only Au and a slight amount of C are present. The EDS shows Au as well as Cu from the nearby support grid.

Figures 6a and 6b show the Au elemental maps obtained using EDS and EELS, respectively. In the case of EDS, the elemental map shows the intensities of the Au M_α line at 2.12 keV extracted using the fitting procedure defined above. The

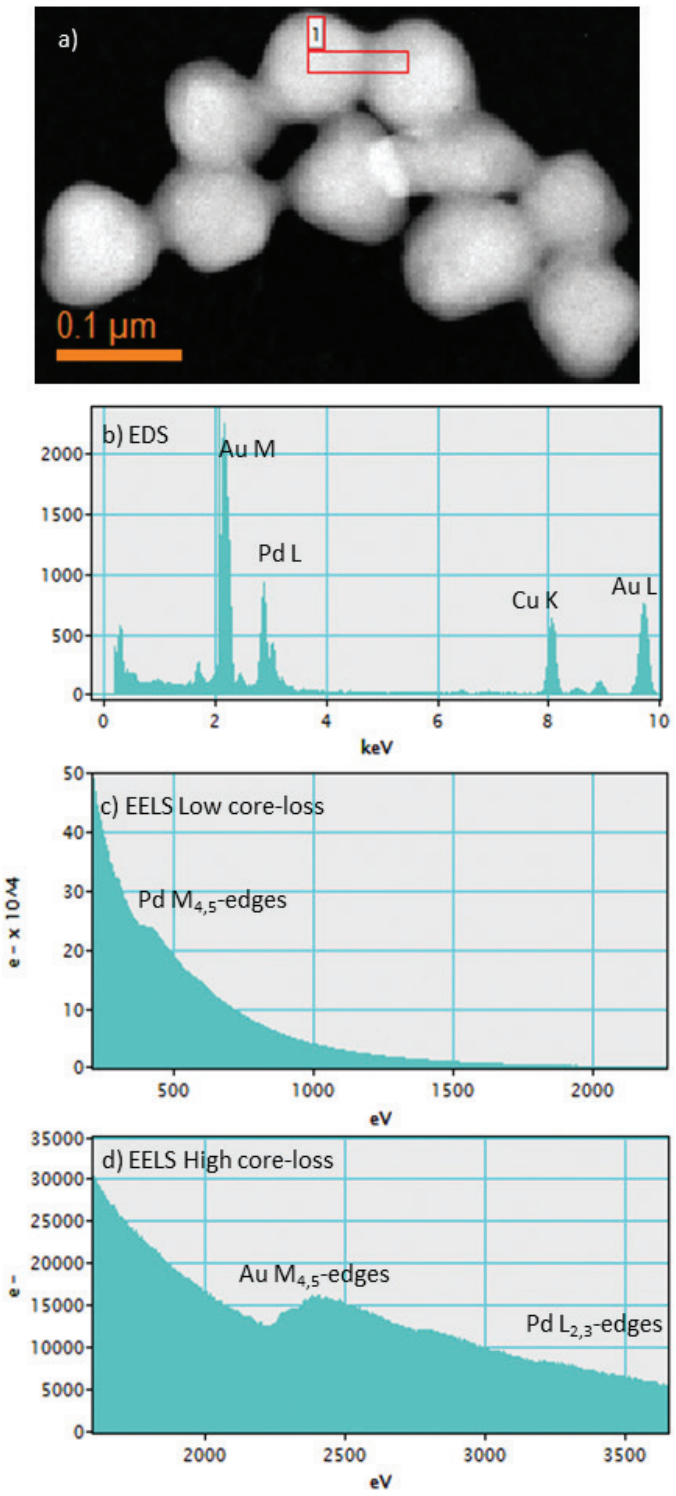

Figure 3: (a)–(d) Same data as Figure 2 but for the summation of 168 adjacent pixels containing both Au and Pd.

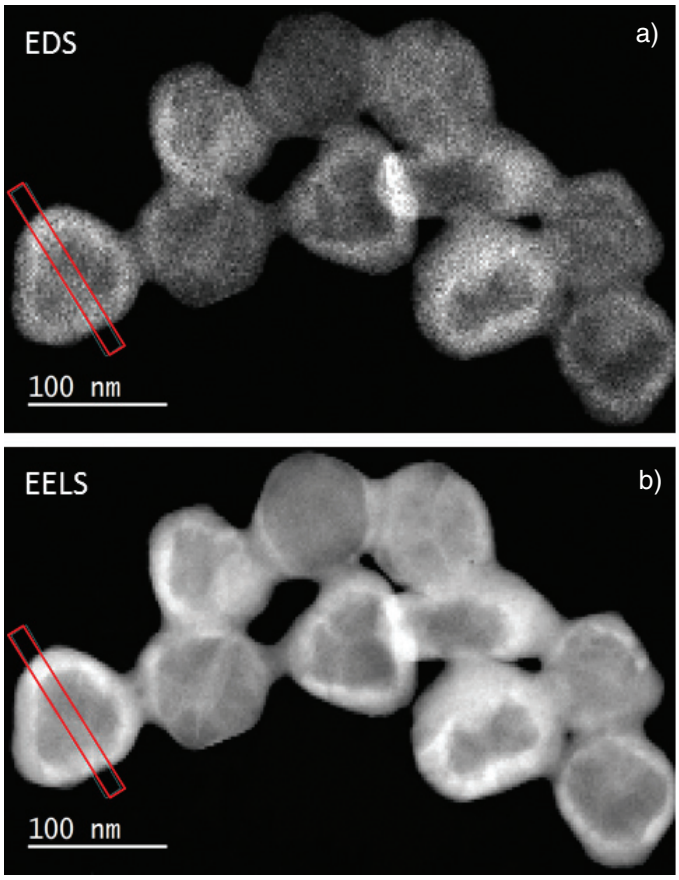

Figure 4: Pd elemental maps. (a) EDS and (b) EELS. The area in the red box is where the intensity line profiles in Figure 5 were extracted.

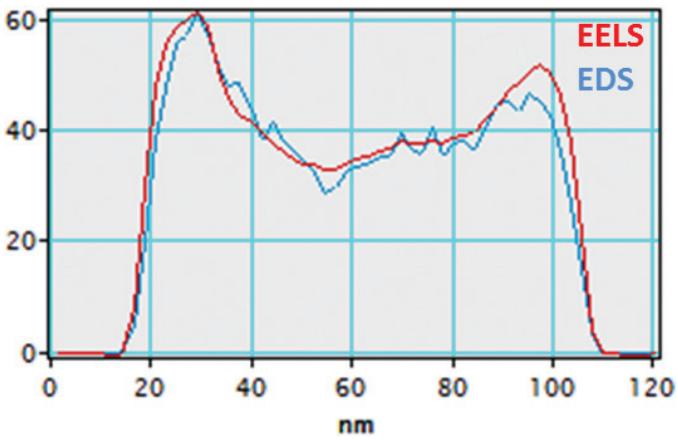

Figure 5: Intensity line profiles extracted from the region in the red box in the Pd elemental maps obtained using EDS and EELS (see Figure 4). Lines were superimposed and normalized to the same maximum.

EELS Au $M_{4,5}$-edges at 2206 eV were extracted using power law background fitting [15]. For the short collection time per pixel, the EELS elemental map for Au shows more details compared to that from EDS, despite the copious flux of X rays from a heavy element such as Au.

To measure the relative quality of each type of map, the signal intensity was analyzed from a uniform region of an Au particle. This 16 × 16 pixel region is shown by the red box in Figure 6, and the extracted data is summarized in Table 1. Here a special statistical function available in DigitalMicrograph was used to measure the mean signal and the standard deviation across the selected area within the 16 × 16 pixel region. The ratio between the mean and the standard deviation would give the SNR. The SNR for the EELS data is ~17, whereas that for the EDS data is ~8 indicating a 2× improvement for the EELS data. Increasing either the

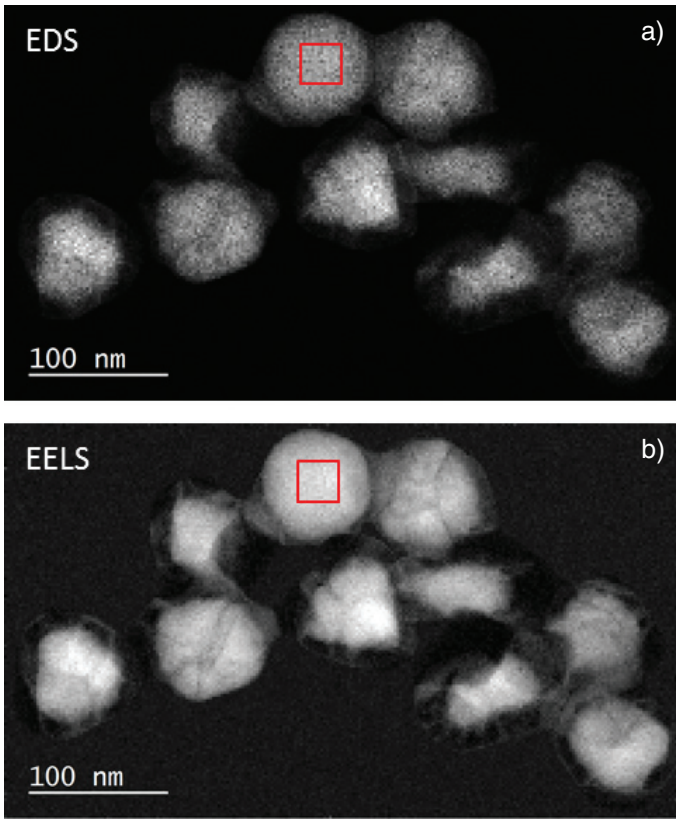

Figure 6: Au elemental maps. (a) EDS and (b) EELS. The red box indicates the area used to calculate the map signal-to-noise ratios.

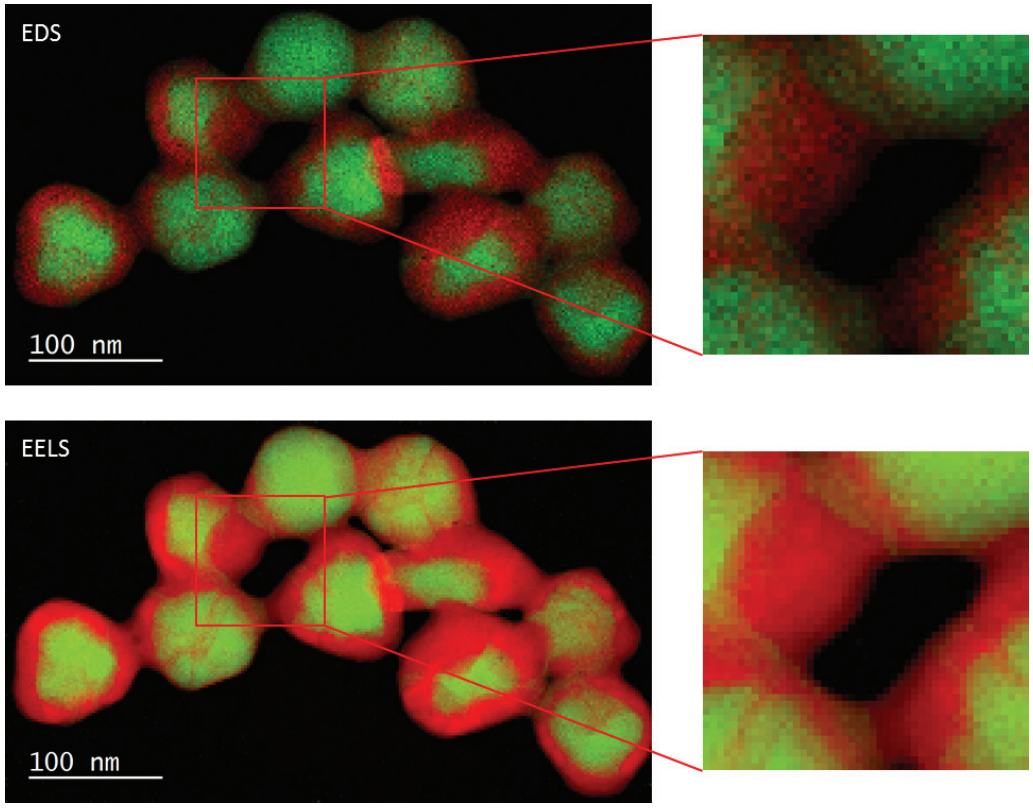

Figure 7: Colorized elemental maps of Pd in red and Au in green acquired using EDS and EELS. The inset is the enlarged image of the region in the red box.

Table 1: Signal-to-noise ratio measurements.

	Mean Signal	Std. Dev.	SNR
Au M EELS Map	14468 counts	856 counts	17:1
Au M EDS Map	79.9 counts	10.1 counts	7.9:1

collection efficiency or the dwell time for the EDS signal by a factor of 4 is required to match the EELS signal in this dataset.

Figures 7a and 7b show colorized elemental maps of Pd and Au obtained using EDS and EELS, respectively. Qualitatively, the EELS maps appear to be sharper and show higher contrast. In particular, significant details are absent in the EDS maps which are clear in the EELS maps. For example, the diffusion of the Pd into the Au region is difficult to discern in the EDS maps, whereas this appears to be clear in the EELS maps.

Discussion

The EELS and EDS data can be regarded as highly complementary. The main difference is that for the EDS case, each pixel carries little information because of the low signal-to-noise ratio of the data even at these long exposure times and with high fluorescence yield materials. However, the high DQE of the EDS technique allows summation of adjacent data almost indefinitely. Adjacent pixel summation improves the spectral quality as the square root of the number of pixels summed at the expense of reducing spatial information. The EELS data, on the other hand, has very high collection efficiently resulting in high signal-to-noise ratios for each pixel acquired. Summing adjacent pixels improves the detection limits considerably but will show diminishing returns once the shot noise in the signal integral becomes irrelevant compared to the increased detector readout noise caused by summation [1, 13, 16].

The techniques further complement each other when identifying artifacts in the data. For example, secondary fluorescence and preferential absorption in the EDS data can be determined from the EELS data, while possible missing elements in the EELS data range acquired can be identified in the summed EDS signal.

Conclusions

A system for fast and efficient acquisition of both EELS and EDS spectra allows the routine collection of both of these complementary data signals. There is no longer a need to choose between analytical techniques; both EELS and EDS can be acquired easily with every data run. The data presented here show the complementary nature

of having both high signal-to-noise and high signal-to-background data acquired at the same location at the same time. Further, the ability of combining composition measurements from EELS and EDS with physical and electronic information also available only from EELS (for example, plasmonic, bandgap, and density of states information) promises to open completely new avenues of materials analysis.

Acknowledgments

Particular acknowledgements go to Jianfang Wang's group at the Chinese University of Hong Kong for kindly providing the TEM specimen used for the experiment; also to Professor Gerald Kothleitner for letting us use his facilities.

References

[1] RD Leapman and JA Hunt, *Microsc Microanal M* 2 (1991) 231–44.
[2] DA Muller, L Fitting Koukoutis, M Murfitt, JH Song, HY Hwang, J Silcox, N Dellby, and OL Krivanek, *Science* 319 (2008) 1073–76.
[3] AJ Gubbens, M Barfels, C Trevor, RD Twesten, PJ Thomas, N Menon, B Kraus, C Mao, and B McGinn, *Ultramicroscopy* 110 (2010) 962–70.
[4] P Schlossmacher, DO Klenov, B Freitag, and HS von Harrach, *Microscopy Today* 18 (2010) 14–20.
[5] J Scott, PJ Thomas, M Mackenzie, S McFadzean, AJ Craven, and WAP Nicholson, *Ultramicroscopy* 108 (2008) 1586–94.
[6] P Longo, RD Twesten, and PJ Thomas, *Microscopy Today* 20 (2012) 30–36.
[7] MS Chen, K Luo, T Wei, Z Yan, D Kumar, C-W Yi, and DW Goodman, *Catal Today* 117 (2006) 37–45.
[8] M Legawiec-Jarzyna, A Srebowata, and Z Karpinski, *React Kinet Cataly Lett* 79 (2003) 157–63.
[9] MS Chen, D Kumar, C-W Yi, and DW Goodman, *Science* 310 (2005) 291–93.
[10] C-W Yi, K Luo, T Wei, and DW Goodman, *J Phys Chem B* 109 (2005) 18535–40.
[11] P Longo, Gatan Inc., *Applications Note 2011*: http://www.gatan.com/files/PDF/Fast_simul_acquisition_EELS_FL.pdf
[12] E Lifshin, *Proc. 9th Ann. Conf. Microbeam Analysis Soc.*, Ottawa, Canada, 1974, p. 53.
[13] K Riegler and G Kothleitner, *Ultramicroscopy* 110 (2010) 1004–13.
[14] RD Leapman and CR Swyt, *Ultramicroscopy* 26 (1998) 393–403.
[15] P Thomas, Gatan Inc., *Knowhow*, December 14, 2006: http://www.gatan.com/resources/knowhow/kh14-spectral.php
[16] RF Egerton, *Electron Energy-Loss Spectroscopy in the Electron Microscope*, Springer, New York, 2011, pp 91–94 and 340–46.

MT

HALF-PAGE ADVERTISEMENT